DOI: 10.61782/fa.2025.0574

FORUM ACUSTICUM
EURONOISE 2025

MODEL-BASED AURALIZATION OF VIBRO-ACOUSTIC METAMATERIAL PARTITIONS

Lucas Van Belle[1,2*] **Fabio Di Giusto**[1,2] **Elke Deckers**[2,3]
[1] Department of Mechanical Engineering, KU Leuven, Belgium
[2] Flanders Make@KU Leuven, Belgium
[3] Department of Mechanical Engineering, Campus Diepenbeek, KU Leuven, Belgium

ABSTRACT

Vibro-acoustic metamaterials have recently emerged as possible lightweight and compact solutions with favorable noise insulation properties. By adding resonant structures on a subwavelength scale to a partition, targeted frequency ranges of strongly reduced sound transmission can be achieved. Although this makes them appealing for reducing band-limited and tonal noise, other noise characteristics and our perception thereof also impact our well-being and health beyond just noise levels. Furthermore, the unconventional frequency content changes caused by vibro-acoustic metamaterials was recently found to possibly lead to more annoyance than conventional solutions.

While the sound perception impact of these metamaterials is yet to be understood, the opportunity arises to include sound perception in their modeling and leverage these insights already in the early design stage. However, full-scale models of these often intricate structures may pose computational challenges. Hence, in this work, a filter-based auralization approach is proposed to enable efficiently predicting and evaluating the impact of metamaterial partitions on the transmitted sound. Analytical model-based filters are derived for single and double metamaterial partitions. Following an experimental verification, a virtual reality demonstrator is set up as an example of an immersive virtual metamaterial design space.

Keywords: *metamaterials, sound transmission, auralization*

**Corresponding author*: *lucas.vanbelle@kuleuven.be.*

1. INTRODUCTION

In the past decades, an intensifying search for innovative compact and lightweight noise and vibration solutions has grown. In this search, vibro-acoustic metamaterials have recently shown great potential due to their unconventional properties, going beyond the possibilities of conventional materials [1, 2]. Vibro-acoustic metamaterials consist of a flexible host structure with sub-wavelength added structural resonant inclusions, which allows creating stop bands – frequency ranges of strong vibration and noise reduction (Fig. 1). This makes them appealing for noise control engineering, in particular for band-limited and tonal noise, especially in the usually hard-to-address low frequency range.

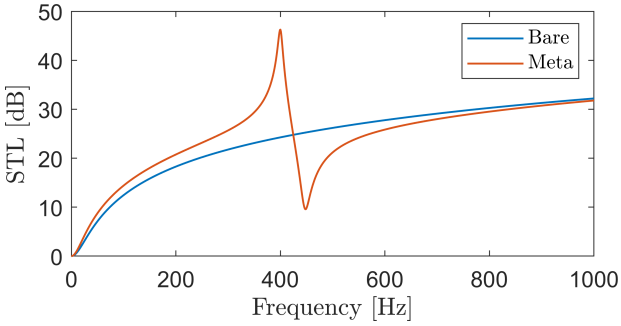

Figure 1. Typical Sound Transmission Loss (STL) curve of an infinite bare homogeneous panel, and a vibro-acoustic metamaterial counterpart targeting the frequency range around 400 Hz.

Various metamaterial concepts have emerged to improve sound insulation of enclosures [3], single panel partitions [4], and double panel partitions [5, 6]. With these

metamaterials, strong noise level reduction is typically pursued, exceeding conventional solutions or improving host structure shortcomings (e.g. the mass-spring-mass resonance in sandwich panels [6]). However, metamaterials can underperform at other frequencies outside the targeted band(s), e.g. the noise insulation dip in Fig. 1. Additionally, the unconventional frequency content changes caused by these metamaterial may not only influence noise levels but also sound perception, possibly even creating more annoyance despite lowering noise levels [7].

While various metamaterial modeling methods exist to predict their stop bands and acoustic insulation performance, only first steps are being taken in predicting [8] and assessing [9] their sound perception impact. Hence, this work proposes an analytical model-based auralization approach, incorporating the fundamental metamaterial tuning parameters, that enables listening to the impact of metamaterial partitions for a given noise signal from the early design stages.

In what follows, first the partitions under consideration are briefly described in Section 2. Next, the sound transmission modeling and filtering-based auralization approach are explained in Section 3. The methodology is applied to a metamaterial foam core sandwich panel, and deployed in a Virtual Reality (VR) demonstrator in Section 4. The main conclusions are summarized in Section 5.

2. PROBLEM DESCRIPTION

This work considers the sound transmission through both single panel partitions as well as double panel partitions with elastic interlayer (Fig. 2).

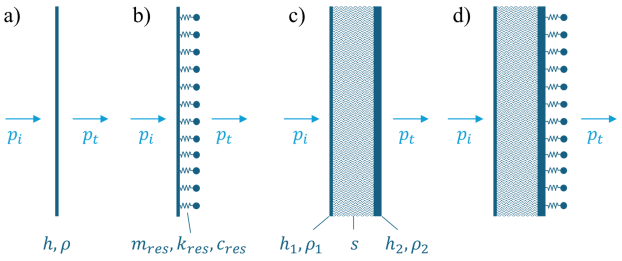

Figure 2. Single wall partition (a) without and (b) with resonant additions. Double wall partition with elastic interlayer (c) without and (d) with resonators.

The panels in these partitions are considered thin, with thickness h and mass density ρ, and the elastic interlayer in the double panel partitions is assumed locally reacting, with stiffness s. From these host structure configurations, metamaterial counterparts are derived by considering mass-spring(-damper) resonators, with mass m_{res}, stiffness k_{res} and damping c_{res}, added to the panels on a sub-wavelength scale (Fig. 2b and d).

3. METHODOLOGY

In order to create audible impressions of the sound transmission through metamaterial partitions, filter functions will be defined based on simplified sound transmission modeling. To this end, an abstraction is made of the possibly many complex vibro-acoustic interactions and environments, and the modeling is simplified to infinite partitions and normal incidence. In particular, the effect of the resonant additions is accounted for via the (equivalent) mass density of the panel to which they are attached. Such simplifications are considered reasonable, since resulting STL predictions have been validated for various single panel [4, 10] and double panel [5, 6] metamaterial partitions.

In the following sections, first the sound transmission model for the single and double panel partition are introduced. Next, the introduction of the metamaterial effect is discussed, after which the filtering approach for auralization is briefly explained.

3.1 Single panel partition

Consider an infinite thin single panel partition subjected to a normally impinging plane wave (Fig. 2a). In air with speed of sound c_0 and mass density ρ_0, the sound pressure transmission coefficient τ relating the transmitted sound pressure p_t to the incident pressure p_i is given by [11]:

$$\tau = \frac{p_t}{p_i} = \frac{2Z_0\omega}{\mathrm{j}2Z_0\omega - \rho h\omega^2}, \tag{1}$$

with the specific impedance of air $Z_0 = \rho_0 c_0$, angular frequency $\omega = 2\pi f$, and frequency f. From this τ, the STL follows as:

$$\mathrm{STL} = -20\log_{10}\left(|\tau|\right). \tag{2}$$

The above expression captures the so-called *mass law* [11], which provides a good approximation of the acoustic insulation behaviour below coincidence. Conventional noise insulation solutions for single panel partitions rely on increasing the panel's mass to increase its STL.

3.2 Double panel partition

Now consider an infinite double panel partition, composed of two thin panels and an elastic interlayer, again subjected to a normally impinging plane wave (Fig. 2c). Besides the mass of the two panels, the coupling stiffness s will have an important effect on the sound transmission behaviour. Following [12, 13], and assuming the frequency range of interest lies far below coincidence, this system can be represented by two plates connected by distributed uncoupled springs, with a sound pressure transmission coefficient given by:

$$\tau = \frac{2Z_0\omega s}{(-\rho_1 h_1\omega^2 + s + \mathrm{j}\omega Z_0)(-\rho_2 h_2\omega^2 + s + \mathrm{j}\omega Z_0) - s^2}. \tag{3}$$

Damping of the elastic interlayer is accounted for by considering a complex-valued s, multiplying with $(1+\mathrm{j}\eta)$ and η the damping loss factor of the interlayer. For an elastic layer with Young's modulus E_{layer} and thickness h_{layer}, the layer's stiffness is obtained as $s = E_{layer}/h_{layer}$.

A key frequency for double panel partitions is the mass-spring-mass resonance frequency f_{mkm} [11]:

$$f_{mkm} = \frac{1}{2\pi}\sqrt{s\left(\frac{1}{\rho_1 h_1} + \frac{1}{\rho_2 h_2}\right)}. \tag{4}$$

Above this frequency, both panels are decoupled, increasing the STL beyond the individual panel mass laws. Below this frequency, the STL follows the mass law of the combined panel masses. Around f_{mkm}, τ becomes high, and the STL is greatly reduced. Metamaterials have shown great potential for targeting this f_{mkm} dip [5, 6].

3.3 Metamaterial partition

Metamaterials enable going beyond the mass law of conventional panels. Hence, an often used strategy to account for the stop band induced sound insulation improvement of metamaterial partitions is to adapt the sound pressure transmission frequency response functions of the host panel with an equivalent mass density ρ_{eq} [14]:

$$\rho_{eq} = \rho + \frac{1}{Sh}\left(\frac{m_{res}(k_{res} + \mathrm{j}\omega c_{res})}{k_{res} + \mathrm{j}\omega c_{res} - \omega^2 m_{res}}\right) \tag{5}$$

for a single resonator per unit cell with area S, or for multiple (n) resonators per unit cell:

$$\rho_{eq} = \rho + \frac{1}{Sh}\sum_{i=1}^{n}\frac{m_{res,i}(k_{res,i} + \mathrm{j}\omega c_{res,i})}{k_{res,i} + \mathrm{j}\omega c_{res,i} - \omega^2 m_{res,i}}. \tag{6}$$

In these equations, the dynamic mass of the resonator(s), which are modeled as mass-spring-damper system(s), is added to the mass of the host structure unit cell. E.g. for a metamaterial single panel partition, filling in Eqn. (5) into Eqn. (1) gives:

$$\tau = \frac{2Z_0\omega}{j2Z_0\omega - \left(\rho + \frac{1}{Sh}\left(\frac{m_{res}(k_{res}+\mathrm{j}\omega c_{res})}{k_{res}+\mathrm{j}\omega c_{res}-\omega^2 m_{res}}\right)\right)h\omega^2}. \tag{7}$$

The m_{res} and k_{res} result from the targeted resonator's eigenfrequency f_{res} and relative mass addition m_{ratio} to the host structure:

$$m_{res} = Sh\rho m_{ratio} \qquad k_{res} = m_{res}(2\pi f_{res})^2. \tag{8}$$

To obtain lumped parameter resonator properties for practically realizable resonators, the possible coupling with the compliance of the host structure can for instance be accounted for by determining f_{res} for a simply supported unit cell with resonator [10], or by computing the dispersion curves for such unit cell and considering the lower stop band edge [5]. In addition, the Modal Effective Mass MEM (in %) of the resonator mode of interest can be accounted for by adapting the resonator mass:

$$m_{res} = Sh\rho m_{ratio} MEM, \tag{9}$$

and by also replacing the mass density ρ of the partition in Eqn. (5) or Eqn. (6) by:

$$\rho' = \rho(1 + m_{ratio}(1 - MEM)), \tag{10}$$

where ρ' now also includes the non-resonant mass added by the resonator to the panel.

3.4 Auralization

To render audible impressions of the transmitted sound through a partition, for a given time-domain excitation $p_{in}(t)$ with time t, the sound pressure transmission coefficients τ are used as a filter function. With the assumption of a linear time invariant system, this filtering can happen both in time or frequency domain [15]. In frequency domain, filtering becomes a straightforward multiplication with τ:

$$p_{out}(\omega) = \tau p_{in}(\omega), \tag{11}$$

whereby the frequency spectrum $p_{in}(\omega) = \mathscr{F}\{p_{in}(t)\}$ of the excitation signal is obtained by taking its Fourier transform. Using the inverse Fourier transform, the filtered pressure time response is recovered as $p_{out}(t) =$

$\mathscr{F}^{-1}\{p_{out}(\omega)\}$ and can be written to an audio file for listening. Note that the same can be obtained via convolution of $p_{in}(t)$ with the impulse response $\tau(t) = \mathscr{F}^{-1}\{\tau(\omega)\}$.

Instead of considering the excitation source signal for $p_{in}(t)$, also the measured acoustic response of an untreated bare panel $p_{bare}(t)$ can be filtered with the difference in sound transmission provided by the metamaterial design, to auralize the response of the metamaterial counterpart $p_{meta}(t)$. In frequency domain, this becomes:

$$p_{meta}(\omega) = \frac{\tau_{meta}}{\tau_{bare}} p_{bare}(\omega) = \tau_{delta} p_{bare}(\omega), \quad (12)$$

with τ_{delta} the difference filter.

4. RESULTS

In this section, the above approach is first experimentally validated for a manufactured metamaterial sandwich panel. Next, an application of the filter-based auralization approach in a VR demonstrator is showcased.

4.1 Metamaterial foam core sandwich panel

In [6], a metamaterial sandwich panel was designed (Fig. 3) to address the low sound insulation at the host structure's f_{mkm}, and its sound insulation performance was experimentally validated. For the host structure composed of an MDF (panel 1), styrofoam (elastic interlayer) and MDF + plasterboard (panel 2) layer, with relevant parameters listed in Tab. 1, $f_{mkm} = 955$ Hz. PMMA beam-shaped cantilever resonators tuned to 1160 Hz were added to panel 1 on a rectangular grid of 40×38 mm, increasing the sandwich panel mass with 8% (Fig. 3, right).

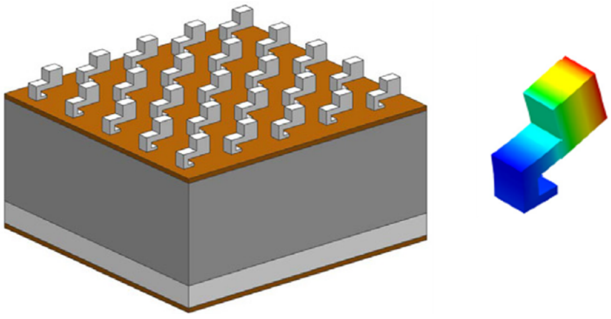

Figure 3. Metamaterial foam core sandwich panel with add-on beam-shaped resonators, tuned with their first out-of-plane bending mode [6] to the mass-spring-mass resonance.

Table 1. Relevant properties of the sandwich panel host structure [6].

	E [MPa]	ρ [kg/m^3]	h [mm]
MDF	3534	765.5	3.3
Plasterboard	1969	766.7	12.5
Styrofoam	5.4	16.83	71.7

As expected, the measured Sound Pressure Level (SPL) for broadband white noise excitation of an A2-sized bare panel mounted on an in-house sound transmission test cabin (Fig. 4) clearly reveals a high SPL peak around the $f_{mkm} = 955$ Hz (Fig. 5).

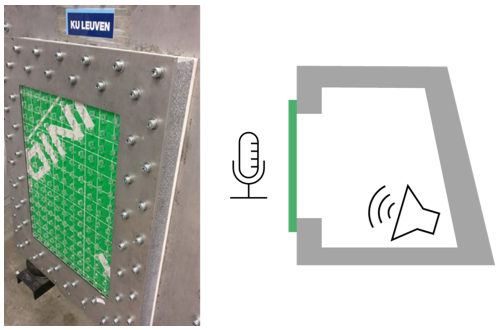

Figure 4. Metamaterial sandwich panel installed on an in-house sound transmission test cabin [6]. A speaker inside the cabin excites the panel, a microphone measures the sound pressure outside the cabin at 1 m in front of the panel center.

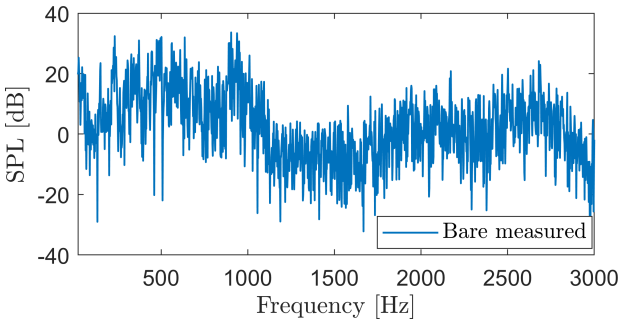

Figure 5. Measured SPL spectrum for the bare, untreated sandwich panel.

Filling the values from Tab. 1 in Eqn. (3), and including a damping loss factor of $\eta = 0.087$ for the foam interlayer as characterised in [6], leads to a normal incidence STL (Fig. 6) which indeed shows the clear low-frequency dip corresponding to the f_{mkm} of the sandwich panel.

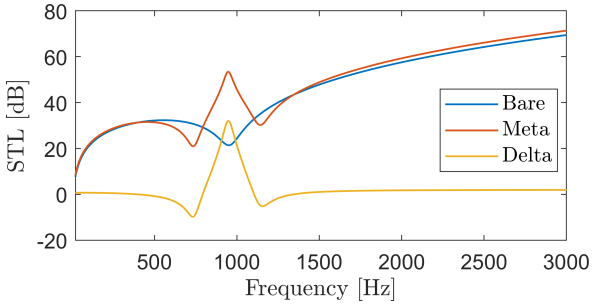

Figure 6. Computed STL for the bare and metamaterial sandwich panel, as well as the STL difference.

For the metamaterial panel, the mass density ρ_1 of panel 1 is adapted using Eqn. (5). To this end, $S = 40 \times 38$ mm^2 , $m_{ratio} = 0.525$ of the resonator w.r.t. panel 1 and, accounting for the flexibility of the host structure [6, 10], $f_{res} = 947$ Hz are considered in Eqn. (8). In addition, $c_{res} = 0.05$ and the mass effectivity of the resonator and its tuned mode is accounted for in Eqn. (9) and Eqn. (10), considering $MEM = 0.5116$ [6, 10]. The resulting modeled STL for the metamaterial panel now shows a high STL peak around the targeted problem frequency, at the expense of two smaller STL dips before and after (Fig. 6), corresponding to the predictions in [6]. The STL difference, corresponding to Eqn. (12), illustrates the strong sound insulation gain enabled by the metamaterial.

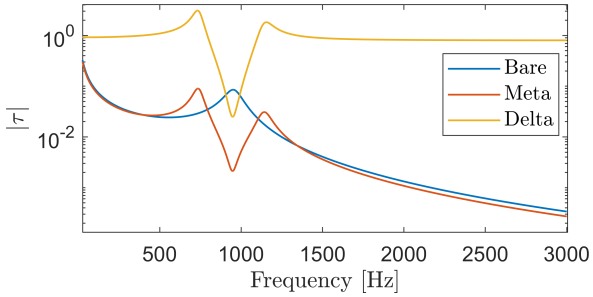

Figure 7. Magnitude of sound pressure transmission coefficients computed for the bare and metamaterial sandwich panel, and for the transmission coefficients difference filter.

For the underlying sound pressure transmission filters τ for the bare and metamaterial partitions in Eqn. (11), as well as the corresponding difference filter τ_{delta} in Eqn. (12) (Fig. 7), the frequency regions of high STL improvement translate to a range of strong sound transmission reduction.

To validate the filter-based auralization approach for the metamaterial effect, the difference filter τ_{delta} is now applied to the sound pressure measurement p_{bare} of the bare partition following Eqn. (12) and compared to the measured sound pressure for the metamaterial partition. Corresponding to [6], the measured SPL spectra of the bare and metamaterial partition (Fig. 8) clearly show a strong reduction around f_{res} and thus the targeted frequency range. Comparing the measured and computed filtered spectrum for the metamaterial partition, very good agreement is observed, although some differences exist.

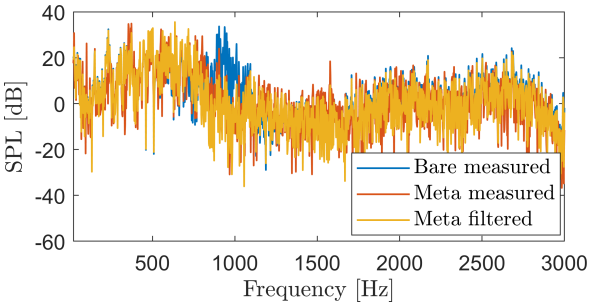

Figure 8. Measured and filtered SPL spectra for the bare and metamaterial sandwich panels.

More interestingly, the measured and auralized sound signals can be listened to (Fig. 9). Comparing the measured responses, the metamaterial stop band (Fig. 9b) clearly filters out an audible dominant peak for the bare sandwich panel (Fig. 9a), seemingly lowering the pitch of the sound. This qualitative change in the transmitted sound is well captured with the auralized metamaterial response (Fig. 9c). This good agreement is also evident in the time-averaged noise level (Fig. 10).

Some discrepancies remain, both in time signals and frequency spectra, which can be attributed to the simple modeling of the partition, the resonators, and the acoustic environment. Nevertheless, a good audible impression of the fundamental metamaterial effect can be achieved, which may provide a powerful means to tailor metamaterial solutions towards adequate noise level reduction and sound quality improvement, from the early design phases.

(a) (b) (c)

Figure 9. Listen to the measured transmitted sound for the bare (a) and metamaterial (b) sandwich panels, and the auralized transmitted sound for the metamaterial sandwich panel (c) (headphones advised).

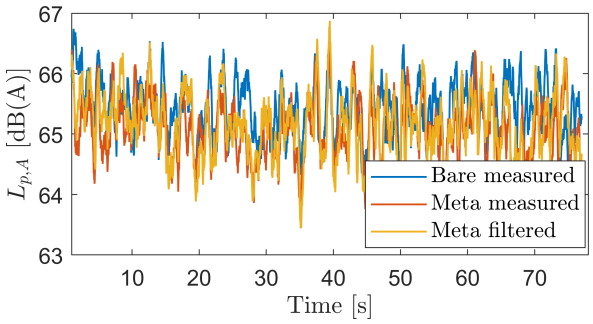

Figure 10. Time-averaged A-weighted sound level $L_{p,A}$ of the measured sound of the bare and metamaterial sandwich panel, and of the filtered sound generated for the metamaterial sandwich panel.

4.2 VR demonstrator

A VR demonstrator has been developed to showcase the benefit which auralization of metamaterial solutions can bring in the early design stage (Fig. 11). To increase audiovisual immersion and realism, the VR demo furthermore implements numerically computed Head-Related Transfer Functions (HRTFs) [16].

The VR demo is designed to render the acoustic effect of sound attenuation for a tonal noise source, by enclosing it with different small enclosures of the same total mass: a bare box, a metamaterial box, and a tunable metamaterial box. In the current implementation, for each enclosure, filtered noise signals are pre-computed off-line. The tonal noise signal exhibits a strong peak around 50 Hz, and at multiples of this fundamental frequency (Fig. 12).

Although metamaterials are very appealing for narrowband noise problems, the multiple harmonics may make appropriate design of (multiple) stop bands challenging, due to perceptual effects. In this case, a metamaterial enclosure with a stop band around 50 Hz and 100 Hz is considered. To auralize its effect, the transmission coefficient for a metamaterial single panel partition with two resonators in Eqn. (5) is used. Compared to an equivalent mass bare single panel partition, the resulting filtered SPL spectrum (Fig. 12) clearly shows the strongly reduced SPL peaks at 50 Hz and 100 Hz.

While attenuating the first two harmonics also clearly benefits the time-averaged noise level (Fig. 13), especially the auralized noise reduction effect provides the designer with a good first impression of the audible beneficial metamaterial effect (Fig. 11). The latter is also made tangible by the third, tunable enclosure, where the user can adapt the tuning of the second stop band frequency and listen to the impact thereof, for the same total enclosure mass.

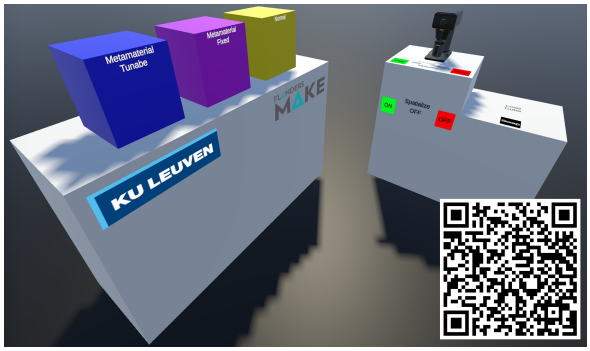

Figure 11. Screenshot of the VR metamaterial demonstrator. The user can listen to a tunable metamaterial enclosure (QR code, headphones advised).

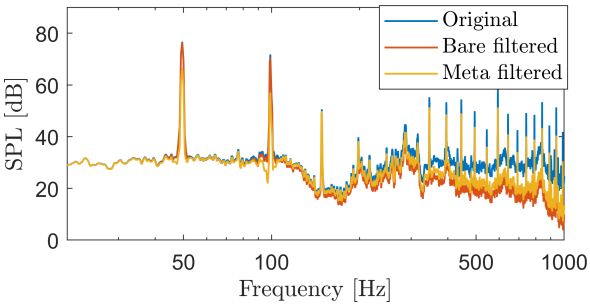

Figure 12. SPL spectra of the original sound, and of the filtered sound generated for the bare (yellow enclosure in Fig. 11) and double stop band metamaterial (magenta enclosure in Fig. 11).

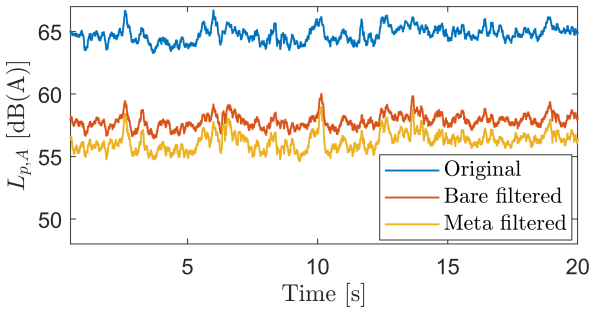

Figure 13. Time-averaged A-weighted sound level $L_{p,A}$ of the original sound, and of the filtered sound generated for the bare (yellow enclosure in Fig. 11) and double stop band metamaterial (magenta enclosure in Fig. 11).

5. CONCLUSIONS

A filter-based auralization approach is proposed to enable efficiently predicting and listening to the impact of metamaterial partitions on transmitted sound, based on analytical sound transmission models of bare and metamaterial single and double panel partitions. The approach was validated on a realized metamaterial sandwich panel, showing good agreement both in terms of spectrum and time signals, but especially also the auralized response. The approach was also applied in a virtual reality demo, further highlighting that model-based auralization of metamaterial partitions may support the early design stages, to assess, adapt and improve noise level and perception effects of metamaterials.

6. ACKNOWLEDGMENTS

The research of L. Van Belle (fellowship no. 1254325N) is funded by a grant from the Research Foundation – Flanders (FWO). Internal Funds KU Leuven are gratefully acknowledged for their support.

7. REFERENCES

[1] Z. Liu, X. Zhang, Y. Mao, Y. Y. Zhu, Z. Yang, C. T. Chan, and P. Sheng, "Locally resonant sonic materials," *Science*, vol. 289, no. 5485, pp. 1734–1736, 2000.

[2] M. I. Hussein, M. J. Leamy, and M. Ruzzene, "Dynamics of phononic materials and structures: Historical origins, recent progress, and future outlook," *Applied Mechanics Reviews*, vol. 66, no. 4, p. 040802, 2014.

[3] C. Claeys, E. Deckers, B. Pluymers, and W. Desmet, "A lightweight vibro-acoustic metamaterial demonstrator: Numerical and experimental investigation," *Mechanical Systems and Signal Processing*, vol. 70, pp. 853–880, 2016.

[4] L. Van Belle, C. Claeys, E. Deckers, and W. Desmet, "The impact of damping on the sound transmission loss of locally resonant metamaterial plates," *Journal of Sound and Vibration*, vol. 461, p. 114909, 2019.

[5] N. G. R. de Melo Filho, L. Van Belle, C. Claeys, E. Deckers, and W. Desmet, "Dynamic mass based sound transmission loss prediction of vibro-acoustic metamaterial double panels applied to the mass-air-mass resonance," *Journal of Sound and Vibration*, vol. 442, pp. 28–44, 2019.

[6] N. G. R. de Melo Filho, C. Claeys, E. Deckers, and W. Desmet, "Metamaterial foam core sandwich panel designed to attenuate the mass-spring-mass resonance sound transmission loss dip," *Mechanical Systems and Signal Processing*, vol. 139, p. 106624, 2020.

[7] L. De Ryck, J. Cuenca, K. Jambrošić, C. Glorieux, M. Rychtarikova, V. Romero-Garcia, A. Cebrecos, N. Jimenez, and J.-P. Groby, "Perceptual evaluation of metamaterials as insulation partitions: A listening test within the cost action denorms (ca15125)," in *Proc. of ISMA2018*, pp. 1147–1161, 2018.

[8] J. Zhang, J. Cuenca, L. De Ryck, L. Van Belle, and E. Deckers, "Impact of design variations of a micro-perforated panel on psychoacoustic metrics of transmitted sound," *The Journal of the Acoustical Society of America*, vol. 156, no. 4_Supplement, pp. A22–A22, 2024.

[9] G. Fusaro, J. Kang, F. Asdrubali, and W.-S. Chang, "Assessment of acoustic metawindow unit through psychoacoustic analysis and human perception," *Applied Acoustics*, vol. 196, p. 108885, 2022.

[10] S. Janssen, L. Van Belle, N. G. R. de Melo Filho, W. Desmet, C. Claeys, and E. Deckers, "Improving the noise insulation performance of vibro-acoustic metamaterial panels through multi-resonant design," *Applied Acoustics*, vol. 213, p. 109622, 2023.

[11] F. J. Fahy, *Sound and structural vibration: radiation, transmission and response*. Academic Press, 2012.

[12] W. Kropp and E. Rebillard, "On the air-borne sound insulation of double wall constructions," *Acta Acustica united with Acustica*, vol. 85, no. 5, pp. 707–720, 1999.

[13] L. Cremer, M. Heckl, and B. A. T. Petersson, *Structure-borne sound: Structural Vibrations and Sound Radiation at Audio Frequencies*. Springer Science & Business Media, 3rd ed., 2005.

[14] Y. Xiao, J. Wen, and X. Wen, "Sound transmission loss of metamaterial-based thin plates with multiple subwavelength arrays of attached resonators," *Journal of Sound and Vibration*, vol. 331, no. 25, pp. 5408–5423, 2012.

[15] J. E. Summers, *Auralization: Fundamentals of acoustics, modelling, simulation, algorithms, and acoustic virtual reality*. Acoustical Society of America, 2008.

[16] Y. Li, J. Cardenuto, F. Di Giusto, S. Preihs, and J. Peissig, "A near-field head-related transfer function data set of kemar with high distance resolution and multiple elevations," in *Proc. of AES 154th Convention*, Audio Engineering Society, 2023.